

# Nanoscale Electrodynamic Response of Nb Superconductors

Tamin Tai\*, Behnood G. Ghamsari, and Steven M. Anlage

**Abstract**—Our objective is to study the extreme and local electrodynamic properties of Niobium (Nb), and to relate these properties to specific defects that limit the ultimate RF performance of superconducting radio frequency (SRF) cavities made from Nb. Specifically, we wish to develop a microscopic measure of the response of Nb to RF magnetic fields up to the critical field ( $H_c$ ) at microwave frequencies (few GHz), and at temperatures down to 4.2 K. In order to image the local electromagnetics response in the GHz frequency regime, a magnetic writer from a commercial hard drive is integrated into the near field microwave microscope and operates with the Nb sample in the superconducting state. The microwave response of Nb thin films from a mesoscopic area are found through linear and nonlinear microwave measurements.

**Index Terms**—Niobium, RF superconductivity, Superconducting materials measurements, Near-field microwave microscope

## I. INTRODUCTION

**B**ASED on the needs of the SRF community to identify defects on Nb surfaces [1], a novel magnetic microscope with the capability of imaging electrodynamic defects in the high frequency regime (at least a few GHz) under a strong RF field up to the thermodynamic critical field of Nb ( $\sim 200$  mT) and at cryogenic temperatures is desirable. A magnetic writer is an excellent candidate for creating strong localized field at high frequencies [2] [3]. Several studies of the high frequency characteristics of the magnetic writer shows that it develops well-confined fields up to a few GHz [3] [4] [5]. An impedance measurement also shows that the writer is well matched to the microwave source over a broad frequency range (2 GHz  $\sim$  25 GHz) [6]. The integration of magnetic writers into our group's microwave microscope also operates successfully at liquid Helium temperature [6] [7]. Therefore the magnetic writer satisfies our need to measure superconductor electrodynamics in the high frequency region. In this paper, we report our experimental results on Nb thin films with thickness 50 nm. We use the magnetic writer to induce the linear microwave response and third harmonic signals from the surface of the Nb thin film, creating response from the linear Meissner effect, the nonlinear Meissner effect, and vortex nonlinearity. The nonlinearity from the Nb vortex critical state shows great potential for high resolution nonlinear imaging to identify defects on Nb cavity surfaces at accelerator operating frequencies and temperatures.

Tamin Tai, B. G. Ghamsari and S. M. Anlage are with Center for Nanophysics and Advance Materials (CNAM), Physics Department, University of Maryland, College Park, MD 20742 USA, (\* e-mail:tamin@umd.edu)

This work is supported by the US DOE/HEP through grant # DESC0004950, and also by the ONR AppEI Center, Task D10, (Award No. N000140911190), and CNAM.

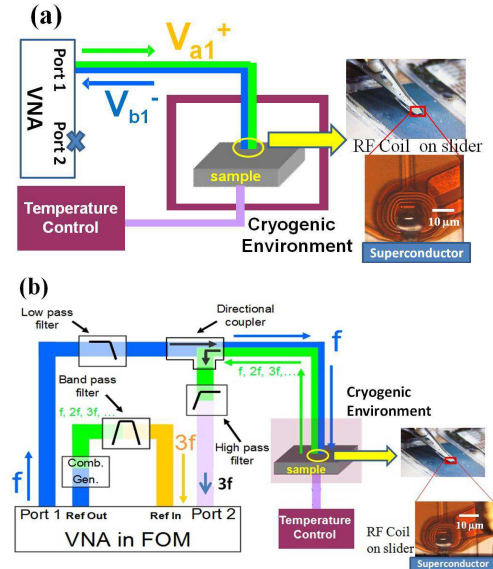


Fig. 1. (a) Schematic diagram of the linear response measurement,  $S_{11}$ , performed as a function of temperature with the (VNA). (b) Schematic set up of phase-sensitive measurement in nonlinear microwave microscopy. Frequency offset mode (FOM) of the VNA is used in this measurement. The microwave circuit inside the cryogenic environment is the same as (a). Only the circuit outside the cryogenic environment is changed for selectively filtering the  $V_{3f}$  signal.

## II. EXPERIMENT

The schematic setup for linear response measurements is shown in Fig. 1(a). A microwave fundamental tone ( $V_{a1}^+$ ) is sent into a Seagate GT5 magnetic writer at one specific frequency from port 1 of the vector network analyzer (VNA) (model # Agilent N5242A). The magnetic writer is designed for longitudinal recording and is integrated into our microwave circuit by soldering the probe assembly on a coaxial cable. The main part of the writer is a yoke surrounded by a several turn helical coil which generates the magnetic flux. The yoke is made of a high permeability material to channel the magnetic flux to the narrow gap. It is also shielded to define a nanoscale bit in the recording medium during the writing process [2]- [5]. Close-up views of the magnetic write head probe on superconducting samples are also shown on the side of Fig. 1. In our design, the magnetic writer approaches the surface of the superconductor in the range of  $200\text{ nm} \sim 2\ \mu\text{m}$ . The fundamental tone stimulates the magnetic writer to generate an RF magnetic field and therefore excites a screening current on the sample surface so that it can maintain the Meissner state in the bulk of the material. Larger magnetic

field induces higher screening current within the penetration depth ( $\lambda$ ) of the superconducting surface, until the field reaches the critical field of the material. The time dependent screening current on the superconductor will induce an electromotive force (emf) on the magnetic writer. The emf voltage will couple with the incident fundamental tone and reflect back as an output signal ( $V_{b1}^-$ ). We measure the ratio of  $V_{b1}^-$  to  $V_{a1}^+$  ( $S_{11}$ ) at different temperatures of the superconducting samples. The sample temperature is controlled by a Lakeshore 340 temperature controller.

The nonlinear amplitude and phase measurements of the superconductor harmonic response utilizes the two-port VNA method shown in Fig. 1(b). An excited wave (fundamental signal) at frequency  $f$  comes from port 1 of the VNA and is low-pass filtered to eliminate higher harmonics of the source signal. This fundamental tone is sent to the magnetic write head probe to generate a localized RF magnetic field on the superconductor sample. The superconducting sample responds by creating screening currents to maintain the Meissner state in the material. These currents inevitably produce a time-dependent variation in the local value of the superfluid density, and will generate a response at harmonics of the driving tone. The generated harmonic signals are gathered by the magnetic probe and returned to room temperature where they are high-pass filtered to remove the fundamental tone  $V_f$ . Finally, an un-ratioed measurement of  $V_{3f}$  is performed on port 2 of the VNA. In order to get a phase-sensitive measurement of the  $3^{rd}$  harmonic signal coming from the superconducting sample, a harmonic generation circuit is connected to provide a reference  $3^{rd}$  harmonic signal, and the relative phase difference between the main circuit and reference circuit is measured. Further detail about this phase-sensitive measurement technique can be found in Ref. [8]. In this way we measure the complex third harmonic voltage  $V_{3f}^{sample}(T)$  or the corresponding scalar power  $P_{3f}^{sample}(T)$ . The lowest noise floor of the VNA in our measuring frequency range is -127 dBm for the un-ratioed power measurement. A ratioed measurement of the complex  $V_{3f}^{sample}(T)/V_{3f}^{ref}$  is also performed at the same time. An alternative method to lower the noise floor is to remove the VNA and use a stable synthesizer (model ‡ HP 83620B) on port 1 and a spectrum analyzer (model ‡: ESA-E E4407B) on port 2. The noise floor of our spectrum analyzer is -147 dBm. The microscope thus measures the local harmonic power and phase generated at the location of the probe, for a given incident frequency, power and sample temperature.

The superconducting samples we study are Nb thin films with thickness 50 nm made by sputtering Nb onto 3 inch diameter quartz wafers. After the deposition, the wafer is diced into many  $10 \times 10 \text{ mm}^2$  pieces but otherwise left un-disturbed. The Nb sample is well anchored to the cold plate to ensure that the surface temperature of the superconductor is the same as the temperature of the cold plate. The probe is held by a three axis translatable stage. Hence different points on the surface of the sample can be examined. We test many pieces from each Nb wafer, and all pieces show consistent results for their linear and nonlinear microwave response.

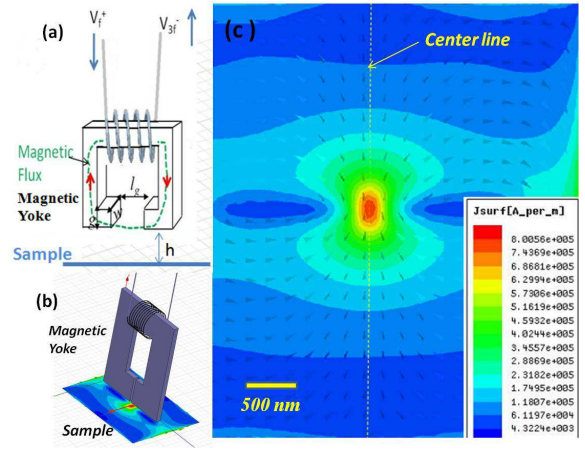


Fig. 2. (a) A schematic magnetic writer and the gap (not to scale) with a height ( $h$ ) away from the sample surface. In our design, we assume  $l_g=100$  nm,  $w=200$  nm, and  $g=1 \mu\text{m}$ . (b) Configuration of HFSS simulation of a magnetic writer above a perfectly conducting sample. (c) Distribution of the surface current density ( $J_{surf}$ ) on the sample surface. The  $J_{surf}$  scale bar and arrows indicate the magnitude and direction of the screening current, respectively, in the first half of the RF cycle. In this simulation, we assume the yoke is made of ferrite. The yoke is excited by a 50 mA RF current and the separation ( $h$ ) between the probe and the sample is 200 nm.

### III. FINITE ELEMENT SIMULATION

The electromagnetic fields produced by the near-field probe on the superconducting surface can be visualized by a finite element simulator, ANSYS High Frequency Structure Simulator (HFSS). Fig. 2 shows the model based on the dimensions of the Seagate GT5 magnetic writer. In this simulation, the sample is assumed to be a perfect electric conductor, not a superconductor. The 10 turn coil is stimulated with a 50 mA drive current at 4.5 GHz excitation frequency. The magnetic flux induced by the incident waves goes out through the gap, about 100 nm long ( $l_g$ ),  $\sim 200$  nm wide ( $w$ ), at the end of the yoke. The thickness of the yoke ( $g$ ) is 1  $\mu\text{m}$ , with a 10 turn gold coil wrapped around it. The sample develops screening currents with a direction perpendicular to the direction of magnetic flux on the sample surface. The screening current on the sample surface has the pattern of a dipole. This screening response is essentially the same as that developed due to a horizontal point magnetic dipole at the location of the gap [9].

The surface magnetic field along the center line, shown as a dashed line in Fig. 2 (c), is plotted in Fig. 3 for different heights ( $h$ ) between the probe and the sample. From the simulation result for a height of 200 nm, the maximum magnetic field ( $B$  field) on the surface is 459.2 mT, higher than the thermodynamic critical field of Nb ( $\sim 200$  mT). It is clear that the closer the probe to the sample, the stronger the magnetic field on the surface. Therefore we want our magnetic writer as close as possible to the sample. The yoke geometry is not quite the same as the simple structure schematically shown in Fig. 2 (a) and (b). Although this simulation cannot describe the GT5 magnetic writer in detail, it provides a general trend and prediction for our microscope.

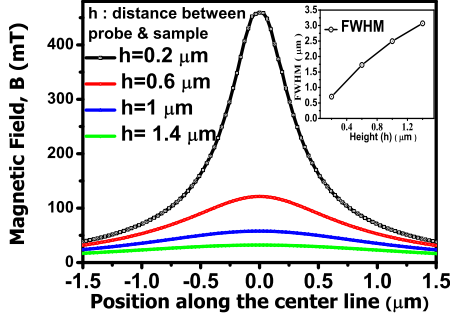


Fig. 3. Magnetic field (B field) on the sample surface calculated by HFSS along the horizontal dash center line on the sample in Fig. 2. The origin of the sample lies exactly below the center of the gap and shows the maximum magnetic field. The calculation is repeated at various heights ( $h$ ) of the probe above the surface. The inset shows the Full Width Half Maximum (FWHM) of the field distribution as a function of height.

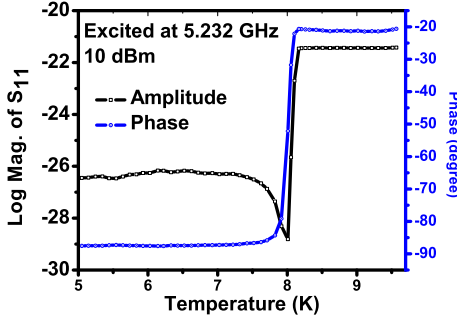


Fig. 4. The temperature dependent  $S_{11}$  of a 50nm Nb thin film measured with the near-field microwave microscope. Both amplitude and phase show a transition at 8.3 K, the same temperature as a global AC susceptibility measurement on this sample.

#### IV. EXPERIMENTAL RESULTS AND DISCUSSION

Many single-position measurements on different 50 nm thick Nb samples were performed. Fig. 4 shows the amplitude and phase of a temperature dependent  $S_{11}$  measurement at a single-position on one of the Nb films under 14 dBm, 5.232 GHz excitation. A sharp change of  $S_{11}$  occurs at 8.3 K for both amplitude and phase. This change indicates the Nb transition temperature ( $T_c$ ). Physically, at this temperature, the Nb thin film becomes superconducting and generates a strong screening current on the sample surface which couples with the incident voltage ( $V_{a1}^+$ ) and results in a change of the reflected voltage ( $V_{b1}^-$ ). In addition, from the normal state to the superconducting state, the surface resistance suddenly drops to a value closer to zero. With a well calibrated measurement and a suitable circuit model for our system, the penetration depth and surface resistance of the superconductors can be extracted from this microwave measurement.

Generally speaking, linear response is not very sensitive to the surface properties. However, for the nonlinear response, the signal will be very sensitive to the surface defects, for example due to defects which generate additional channels of dissipation and reactance. We change our microwave circuit to that in Fig. 1(b) and probe many single points on

the Nb surface. For each point, the magnetic writer probe has to lift, laterally translate to another position and then probe the new position. The height of the probe is judged by optical microscopy and an attempt is made to keep the same height of the probe in each measurement. We see significant differences at different points for this third harmonic nonlinear measurement. A representative result at one point is shown as the dots in Fig. 5. A peak in  $P_{3f}(T)$  near 8.3 K indicates the  $T_c$  of this material and can be interpreted as the intrinsic nonlinearity from the modulation of the superconducting order parameter near  $T_c$  due to the decrease of superfluid density and the associated divergence of the penetration depth near  $T_c$  [8], [10]. Note that a low temperature nonlinearity follows up after the peak and gradually grows while decreasing temperature. This low temperature nonlinearity may come from the Abrikosov or Josephson vortex critical state, and implies a nonlinear mechanism related to moving flux or vortices inside the film [10]. In other words, when the field from the writer is higher than the lower critical field ( $H_{c1}$ ) of the Nb, magnetic flux will penetrate into the superconductor and produce a nonlinear response [11]. This mechanism can be interpreted as at least one vortex (or one vortex/antivortex pair) overcoming the Bean-Livingston barrier [12] and penetrating into the film. In this case, it is not clear how many vortices are involved or the manner of vortex entry and exit; either in the form of a semiloop [13] or perpendicular vortex/anti-vortex pair [14]. However, considering the gap geometry of the magnetic writer probe and the known film thickness, which is comparable to the value of its magnetic penetration depth at zero temperature, a harmonic response from a perpendicular vortex-antivortex pair may be the mechanism of this additional nonlinearity [14].

The solid line in Fig. 5 shows the result of curve fitting to  $P_{3f}$  based on the mechanism of the intrinsic nonlinearity near  $T_c$  using the Ginzburg-Landau (GL) model [15]. The generated third harmonic power  $P_{3f}$  can be estimated as Eq. (1) derived for the time dependent nonlinear inductive circuit [15] [16].

$$P_{3f}(T) = \frac{\omega^2 \mu_0^2 \lambda^4(T) \Gamma^2(K_{RF})}{32 Z_0 d^6 J_{NL}^4(T)} \quad (1)$$

where  $\omega$  is the angular frequency of the incident wave,  $\lambda(T)$  is the temperature dependent magnetic penetration depth,  $d$  is the thickness of the film,  $\mu_0$  is the permeability of free space,  $Z_0$  is the characteristic impedance of the transmission line in the microscope, and  $\Gamma(K_{RF})$  is a probe geometry factor. The probe geometry factor  $\Gamma$  is a function of the induced surface current density,  $K_{RF}$ , which is proportional to the applied magnetic field. The value of geometry factor is estimated to be  $10^5 A^3/m^2$ , calculated from the Karlqvist equation for the magnetic field from a magnetic write gap [17] under the assumption that the probe height is around 2  $\mu m$  above the superconducting surface. The term  $J_{NL}$  is the nonlinear current density scale and quantitatively characterizes the mechanism of nonlinearity. For the intrinsic nonlinearity, this term is on the scale of the de-pairing current density of the superconductor. Based on the GL model, the temperature

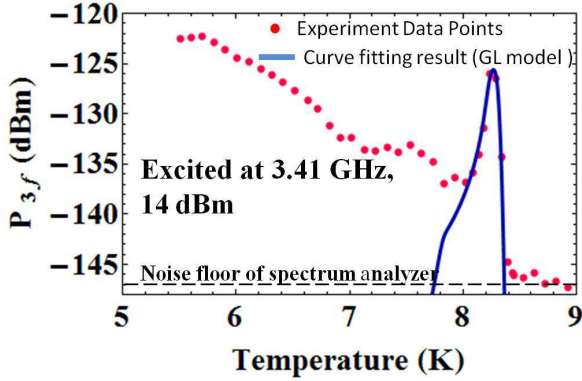


Fig. 5. Temperature dependence of the third harmonic response for a 50 nm thick Nb film. In this measurement, a microwave synthesizer and a spectrum analyzer are used for the nonlinear measurement as port 1 and port 2, respectively on the VNA. The noise floor of the spectrum analyzer in the  $P_{3f}(T)$  measurement is -147 dBm. The dot points are experiment  $P_{3f}$  data. A calculated result (solid curve) based on the GL model is fit to the data near  $T_c$ . The parameters are as follows:  $\Gamma=10^5 \text{ A}^3/\text{m}^2$ ,  $\lambda(0\text{K})=40 \text{ nm}$ ,  $\lambda_{cutoff}=312 \text{ nm}$ ,  $J_{cutoff}=2.1 \times 10^{11} \text{ A}/\text{m}^2$ , and  $T_c=8.3 \text{ K}$  with a standard deviation of Gaussian spread of  $\delta T_c=0.03 \text{ K}$ .

dependent  $J_{NL}(T)$  can be written as

$$J_{NL} = J_0 \left[ 1 - \left( \frac{T}{T_c} \right)^2 \right] \left[ 1 - \left( \frac{T}{T_c} \right)^4 \right]^{1/2} \quad (2)$$

where  $T_c$  is the critical temperature,  $J_0$  is the critical current density at 0 K, which can be estimated as  $H_0/\lambda_0$  where  $H_0$  and  $\lambda_0$  are the thermodynamic critical field and penetration depth of Nb at 0 K, respectively. In our calculation,  $H_0$  is assumed to be 200 mT and  $\lambda_0$  is 40 nm. As T approaches  $T_c$ , the cutoff of  $\lambda(T)$  &  $J_{NL}(T)$  and a Gaussian distribution of  $T_c$  in Eq. (1) are also applied in this calculation. Finally from our result of the curve fitting as shown in the solid curve, this model describes well the experimental results near  $T_c$  and proves that the measured  $P_{3f}(T)$  peak comes from the mechanism of intrinsic nonlinearity. For the low temperature ( $T < T_c$ ) nonlinearity, other mechanisms must be responsible for  $P_{3f}(T)$ .

In order to further understand the complex-valued third harmonic voltage  $V_{3f}$ , the phase-sensitive harmonic technique is performed on the 50 nm thick Nb thin film. In this measurement, the unratified measurement shows a corresponding scalar power  $P_{3f}^{sample}(T)$ , which is analogous to the  $P_{3f}(T)$  measurement done by the spectrum analyzer. Fig. 6 shows a representative curve for this measurement. Note that the probe position in this measurement is different from that of Fig. 5. The red curve is the phase of the complex  $V_{3f}^{sample}(T)/V_{3f}^{ref}$ . The blue curve is the corresponding scalar power  $P_{3f}^{sample}(T)$ . Clearly, the phase shows a minimum at  $T_c$  ( $\sim 8.3\text{K}$ ) while the harmonic magnitude  $P_{3f}(T)$  exhibits a maximum. Note that between the normal state and the superconducting state of Nb, the phase shift is almost  $\pi/2$ , consistent with an analytical model for the harmonic phase variation near  $T_c$  [8]. After this minimum, the phase is followed by a turning point at 8.0 K, which implies a change in the dominant nonlinear mechanism from the intrinsic nonlinearity near  $T_c$  to the nonlinearity in the vortex critical state. For temperatures below 8 K, the phase

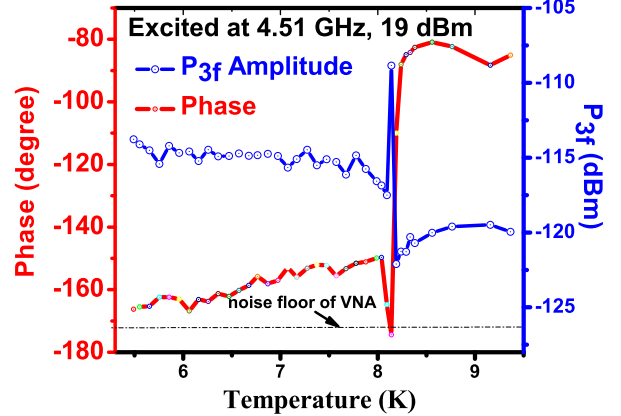


Fig. 6. Temperature dependence of the third harmonic response with amplitude (blue) and its relative phase (red) for a 50 nm thick Nb film. The two-port VNA measurement is used. The noise floor of the VNA in the  $P_{3f}(T)$  measurement is -127 dBm. Note that the temperature scale was corrected because of poor thermal contact of the thermometer.

gradually decreases with decreasing temperatures while the amplitude of the  $P_{3f}(T)$  slightly increases.

Comparing to the  $P_{3f}(T)$  of Fig. 5, there are many similarities and differences. From the  $P_{3f}(T)$  above  $T_c$  in Fig. 6, it is clear that the probe shows some nonlinearity at high excitation power. This nearly temperature independent probe nonlinearity is due to the hysteretic properties of the high permeability material in the yoke [6] and will become significant at high excited power. Therefore at  $T > T_c$ , all of the nonlinearity comes from the probe itself. Both  $P_{3f}(T)$  in Fig. 5 and Fig. 6 show a peak at 8.3 K indicating the  $T_c$  of the Nb thin film. After the peak, both of the temperature dependence of  $P_{3f}(T)$  are consistent with that of Josephson vortices [10]. However, this  $P_{3f}(T)$  behaves a little bit different. We see different levels of  $P_{3f}(T)$  increase with decreasing temperatures at different locations. This may imply that the nonlinearity from the moving vortices is very sensitive to surface morphology and probe-sample separation. For further detailed analysis, a raster scan of the probe should be performed to realize the relation between surface morphology and vortex motion in the vortex critical state.

## V. CONCLUSION

From the linear and nonlinear measurement of Nb thin films by the near field magnetic field microwave microscope, the electrodynamic properties of Nb materials can be identified. The linear response can be used to find the film  $T_c$  in a local area. The third harmonic response shows a nonlinearity likely from the Abrikosov vortex critical state, which implies the magnetic field from the probe is higher than the  $H_{c1}$  of the 50 nm thick Nb thin film. Therefore the nonlinear near-field magnetic field microwave microscope has great potential to image the electrodynamic defects on superconducting Nb in the GHz frequency region.

## REFERENCES

- [1] M. Muck, C. Welzel, A. Farr, F. Schloz, W. Singer, "Nondestructive testing of Niobium sheets for superconducting resonators" *IEEE Trans. Appl. Supercond.*, vol. 13, no. 2, p. 239, June 2003.
- [2] F. H. Liu, S. Shi, J. Wang, Y. Chen, K. Stoev, L. Leal, R. Saha, H.C. Tong, S. Dey, M. Nojaba, "Magnetic recording at a data rate of one gigabit per second," *IEEE Trans. Appl.*, vol. 37, No. 2, pp. 613-618, March 2001.
- [3] W. C. Lin, J. G. Zhu, T Pan, "Measurement of high data rate performance in perpendicular magnetic recording" *J. Appl. Phys.*, vol. 105, p. 07B735, 2009.
- [4] M. Abe, Y. Tanaka, "A study of high frequency characteristics of write heads with the ac-phase high frequency magnetic force microscope," *IEEE Trans. Magn.*, vol.38, p. 45, 2002.
- [5] M. R. Koblischka, J.-D. Wei, T. Sulzbach, A. D. Johnston, U. Hartmann, "Observation of stray fields from hard-disk writer poles up to 2 GHz," *IEEE Trans. Magnetics*, vol. 43, no. 6, p. 2205, 2007.
- [6] Tamin Tai, X. X. Xi, C. G. Zhuang, D. I. Mircea, S. M. Anlage, "Nonlinear near-field microwave microscope for RF defect localization in superconductors," *IEEE Trans. Appl. Supercond.* vol. 21, p. 2615, 2011.
- [7] Tamin Tai, B. G. Ghamsari, S. M. Anlage, "Nanoscale electrodynamic vortex response of Nb superconductors," *CPEM 2012 Digest Tu4-P2-Mg2*, P30, 2012.
- [8] D. I. Mircea, H. Xu, S. M. Anlage, "Phase-sensitive Harmonic Measurements of Microwave Nonlinearities in Cuprate Thin Films," *Phys. Rev. B* **80**, p. 144505, 2009.
- [9] M. V. Milošević, S. V. Yampolskii, and F. M. Peeters, "Magnetic pinning of vortices in a superconducting film: The antivortex magnetic dipole interaction energy in the London approximation," *Phys. Rev. B* vol. 66, p. 174519, 2002
- [10] S. C. Lee, S. Y. Lee, S. M. Anlage, "Microwave nonlinearities of an isolated long  $YBa_2Cu_3O_{7-\delta}$  bicrystal grain boundary" *Phys. Rev. B* vol. 72, p. 024527 2005.
- [11] L. Ji, R. H. Sohn, G. C. Spalding, C. J. Lobb, and M. Tinkham, Critical state model for harmonic generation in high-temperature superconductors, *Phys. Rev. B* vol. 40, pp. 10936-10945 1989.
- [12] C. P. Bean, J. D. Livingston, "Surface barrier in Type-II superconductors," *Phys. Rev. Lett.* vol. 12, pp. 14-16, 1964.
- [13] A. Gurevich, G. Ciovati, "Dynamics of vortex penetration," *Phys. Rev. B* vol. 77, p. 104501, 2008.
- [14] G. Carneiro, "Pinning and creation of vortices in superconducting films by a magnetic diople," *Phys. Rev. B* vol. 69, p. 214504, 2004.
- [15] S. C. Lee, M. Sullivan, G. R. Ruchti, and S. M. Anlage, "Doping dependent nonlinear Meissner effect and spontaneous currents in high- $T_c$  superconductors," *Phys. Rev. B* vol. 71, p. 014507, 2005.
- [16] Sheng-Chiang Lee, "Measurement of doping dependent microwave nonlinearities in high temperature superconductors" *Ph.D Dissertation, University of Maryland-College Park* 2004, <http://hdl.handle.net/1903/1372>.
- [17] S. X. Wang and A. M. Taratorin, "Magnetic Information Storage Technology" San Diego, CA: Academic Press, Chapter 2, p. 38, 1999.